Journal of the Physical Society of Japan **94**, 074703 (2025) **Full Papers**
https://doi.org/10.7566/JPSJ.94.074703

Polarization-dependent Bulk-sensitive Valence Band Photoemission Spectroscopy and Density Functional Theory Calculations: Part IV. 4*f* Rare-earths

Shigenori Ueda[1,2*] and Ikutaro Hamada[3]

[1]*Research Center for Electrical and Optical Materials, National Institute for Materials Science (NIMS), Tsukuba, Ibaraki 305-0044, Japan*
[2]*Synchrotron X-ray Station at SPring-8, NIMS, Sayo, Hyogo 679-5148, Japan*
[3]*Department of Precision Engineering, Graduate School of Engineering, The University of Osaka, Suita, Osaka 565-0871, Japan*

(Received February 4, 2025; accepted May 14, 2025; published online June 11, 2025)

The valence band electronic structures of the elemental solids of 4*f* rare-earths (REs: La, Ce, Pr, Nd, Sm, Eu, Gd, Tb, Dy, Ho, Er, Tm, Yb, and Lu) were studied by bulk-sensitive polarization-dependent hard X-ray photoemission spectroscopy (HAXPES). Owing to the localized 4*f* electrons in REs, the valence band (VB) region showed complicated multiplet structures reflecting the 4*f* photoemission final states, except for La and Ce. The profiles of the 4*f* multiplet structures did not depend on the X-ray polarization. In contrast, the VB spectra, which mainly consisted of the 5*d* and 6*s* states, near the Fermi-level (E_F) weakly depended on the X-ray polarization. The polarization-dependent VB spectra near E_F for La and Lu were reproduced by the 5*d* and 6*s* partial densities of states, which were obtained from the density functional theory calculations for La and Lu, multiplied by photoionization cross-sections. The complicated multiplet structures were also observed in the 3*d* and 4*d* core-level HAXPES spectra via the exchange interaction between the core–hole and 4*f* electrons.

1. Introduction

In the elemental solids of 4*f* rare-earths (REs) or so-called lanthanides (La–Lu), the number of electrons in the 4*f* orbital (n) changes with the atomic number (Z), where n is given by $Z - 57$ ($Z = 57$ for La), except for Eu and Yb ($n = Z - 57 + 1$). Many 4*f* RE elemental solids have a magnetic ground state due to the localized 4*f* orbital as well as elemental solids of 3*d* transition metal (TM), but Curie or Neel temperature (T_C or T_N) of 4*f* REs is lower than room temperature (RT) in contrast to that T_C or T_N of 3*d* TMs such as Cr, Mn, Fe, Co, and Ni is higher than RT. The localized 4*f* electrons in REs have attracted in fundamental physics by means of various high-energy spectroscopies such as photoelectron spectroscopy (PES), inverse PES (called as IPES or BIS: bremsstrahlung isochromat spectroscopy), X-ray absorption spectroscopy (XAS), and electron energy loss spectroscopy (EELS), since complicated multiplet structures have been observed in many REs in these methods.[1)] Valence fluctuation and heavy fermion properties have also attracted in the studies of electronic states of RE alloys and compounds by using PES.[2)] RE-TM intermetallic compounds have been brought into the research field of advanced permanent magnets.[3)] In addition, it is known that some of RE alloys and compounds exhibit catalytic properties[4)] and superconductivity.[5,6)] Thus, 4*f* REs are of importance in fundamental physics and applications.

This paper is a series of X-ray polarization-dependent valence band (VB) hard X-ray PES (HAXPES) studies of elemental solids using 5.95 keV X-rays. HAXPES is well known as a bulk-sensitive probe of the electronic states of solids,[7–10)] since the kinetic energy of photoelectron reaches to several-keV. Such high-kinetic energy photoelectrons have a large inelastic mean-free-path (IMFP) in solids according to the TPP-2M equation.[11)] Therefore, HAXPES enables us to obtain the bulk-sensitive electronic states of solids with less containing surface-related electronic states in a suitable experimental geometry.[12)] In the previous studies, we have shown the experimental polarization-dependent VB HAXPES spectra for 3*d*, 4*d*, and 5*d* TMs with the simulatied results of VB spectra obtained by using the calculated photoionization cross-sections and partial densities of states (PDOSs) based on the density functional theory (DFT) calculations.[13–15)] In this work, we have performed the polarization-dependent VB HAXPES measurements for 4*f* REs of La, Ce, Pr, Nd, Sm, Eu, Gd, Tb, Dy, Ho, Er, Tm, Yb, and Lu elemental solids. The changes in the VB spectral shapes of the band originated from the 5*d*, 6*s*, and 6*p* states showed a clear X-ray polarization dependence mainly due to the photoionization cross-section ratio of 5*d*/6*s* orbitals, which strongly depended on X-ray polarization and experimental geometry.[13)] In contrast, the spectral shapes of multiplet structures due to the $4f^{n-1}$ photoemission final states did not depend on X-ray polarization, which would be attributed to the use of polycrystalline 4*f* RE samples. We have also performed the 3*d*, 4*d*, and 4*s* core-level HAXPES measurements for 4*f* REs as a reference data set. Note that conventional X-ray photoemission spectroscopy (XPS) using Al-Kα (1486.7 eV) or Mg-Kα (1253.6 eV) cannot access to all the 3*d* core-levels in 4*f* REs owing to their high binding energy (830–1650 eV), while all the 3*d* core-level spectra for 4*f* REs are observable in HAXPES at the photon energy of 5.95 keV with higher bulk-sensitivity compared to conventional XPS. The 3*d* and 4*d* core-level HAXPES spectra for 4*f* REs have revealed the complicated multiplet structures due to the c$4f^n$ photoemission final states (c denotes core–hole) because of high-resolution (HR) measurements.

2. Experimental

X-ray polarization-dependent VB HAXPES measurements for 4*f* RE elemental solids were conducted at the undulator beamline BL15XU[9,16)] of SPring-8. The polycrystalline ingots of La, Ce, Pr, Nd, Sm, Eu, Gd, Tb, Dy, Ho, Er, Tm, Yb, and Lu with purity better than 99.9% were in situ fractured to obtain clean surfaces in a sample preparation chamber with the base pressure of 2.0×10^{-7} Pa. Then, the samples were transferred to an analysis chamber, which was equipped with a HR hemispherical electron analyzer (VG

Scienta, R4000), with the base pressure of 3.0×10^{-8} Pa. The temperature of samples was kept at 15 K during the measurements. The photoelectrons were excited by horizontal (H-pol), vertical linear polarized (V-pol) X-rays or left- or right-handed circularly polarized (C-pol) X-rays. A near-normal emission geometry with a grazing incidence (approximately 2°) of X-rays with respect to a nominal sample surface was applied to the HAXPES experiments. The incident X-rays were firstly monochromatized by a Si 111 double-crystal monochromator and then were further monochromatized by a Si 333 channel-cut monochromator. The X-ray polarization was switched by using a diamond phase retarder, while the phase retarder was retracted from the X-ray axis for H-pol X-rays. The estimated degree of linear or circular polarization (P_L or P_C) was ∼1.00, ∼0.70, and ∼0.95 for H-, V-, and C-pol X-rays, respectively. P_L correction to ∼1.00 was done for the VB spectra measured with V-pol X-rays in this work as described elsewhere.[13–15] The VB spectra for C-pol X-rays were obtained by the average of the VB spectra for left- and right-handed C-pol X-rays in each element. The 3*d*, 4*d*, and 4*s* core-level HAXPES measurements were performed with H-pol X-rays. Overall energy resolution (ΔE) of the HAXPES measurements was set to 130 meV, and the binding energy (E_B) was calibrated by the Fermi-level (E_F) of a reference Au film. For Ce and Eu, we have done HR HAXPES measurements of VB and Eu 4*f* states with ΔE = 85 meV.

3. DFT Calculations

DFT calculations were performed to obtain the electronic band structures (total DOS and PDOSs) for La and Lu. The projected augmented method[17] as implemented in the VASP code[18,19] was used. The generalized gradient approximation of Perdew, Burke, and Ernzerhof[20] was applied to the exchange–correlation functional. The experimental structures of La[21] and Lu[22] were used in the DFT calculations: double hexagonal closed pack (dhcp) structure for La and hcp structure for Lu. A kinetic energy cut-off of 750 eV was used to expand the wave functions in terms of a plane-wave basis set. The tetrahedron method was used for the Brillouin-zone integration with the $36 \times 36 \times 12$ and $36 \times 36 \times 24$ *k*-point grids for La and Lu, respectively. We omitted to perform the DFT calculations of the other REs due to the strong final state effects in the partially filled 4*f* states in PES.[23] The spin–orbit coupling was not considered in the DFT calculations for simplicity.

4. Results

4.1 Polarization-dependent VB HAXPES spectra of 4f REs

Figures 1(a)–1(n) shows the polarization-dependent VB spectra of the 4*f* REs of La, Ce, Pr, Nd, Sm, Eu, Gd, Tb, Dy, Ho, Er, Tm, Yb, and Lu. The VB spectra for H-, V-, and C-pol X-rays were normalized by the incident photon intensity in each element, and subtractions of an integrated-type-background were performed. The VB intensity was highest (lowest) for H-pol (V-pol) X-rays in each element and the intermediate VB intensity was found for C-pol X-rays, as well as HAXPES for the elemental solids of 3*d*, 4*d*, and 5*d* TMs.[13–15] The VB spectra were classified into two parts: 5*d*6*sp* hybridized band near E_F and multiplet structures due to 4*f* photoemission final states. For La and Ce, the 4*f* derived structures cannot be found in Figs. 1(a) and 1(b). The absence of 4*f* photoemission in La is natural because of the empty 4*f* orbital ($n = 0$). The absence of 4*f* photoemission in Ce will be mentioned latter. For Yb and Lu, the spin–orbit doublet ($4f_{7/2}$ and $4f_{5/2}$) due to the fulfilled 4*f* orbital ($n = 14$) can be seen in Figs. 1(m) and 1(n). The 4*f* multiplet structures strongly depended on *n*, and were similar to those for 4*f* REs reported in conventional XPS measurements.[23] One sees that the 4*f* multiplet structures in Eu and Gd are similar each other, which is caused by same *n* in the initial state of Eu and Gd. The multiplet structure becomes complicate with increasing *n* up to 13. The assignment of 4*f* multiplet states was described elsewhere.[23,24]

Although the profile of multiplet structure in Figs. 1(c)–1(l), does not depend on the X-ray polarization, the profiles of 5*d*6*sp*-derived band near E_F in Figs. 1(a)–1(n) change with the X-ray polarization. The changes in the 5*d*6*sp*-derived band profile are weak in peak structures (shoulder structure in the case of La) immediately below E_F and are strong in broad peaks located at $E_B \sim 1.5$ eV. According to the previous polarization-dependent HAXPES work for 3*d* and 4*d* TMs,[13,14] the photoionization cross-sections for *s* atomic orbitals abruptly decrease in V-pol X-rays compared to H-pol X-rays in our experimental configuration. Therefore, we see that the 5*d*-derived photoemission intensity is dominant in the observed band profile with a varied contribution of 6*s*-derived one by the X-ray polarization in the HAXPES spectra of 4*f* REs. For Eu and Yb, changes in the observed band profile are unclear, since the band is overlapped with 4*f* photoemission in both cases. A small hump at $E_B \sim 5$ eV shows the X-ray polarization dependence for Eu and Gd in Figs. 1(f) and 1(g), and the intensity of the hump reduces in the case of V-pol X-rays, suggesting that the small hump mainly originates from the 6*s*-derived states. Note that the contribution of 6*p*-derived intensity in 4*f* REs might be quite small by considering the experimental HAXPES results and calculated photoionization cross-sections for 6*p* atomic orbitals in 5*d* TMs.[15]

In Figs. 1(a)–1(n), a metallic Fermi edge was clearly observed in each RE regardless of X-ray polarization. This result indicates that the recoil effect[25–27] in 4*f* RE elemental solids is sufficiently smaller than ΔE = 130 meV. In fact, the calculated recoil energy of photoelectrons with the kinetic energy (E_K) of 5.95 keV for the isolated 4*f* RE atoms according to Refs. 25–27 ranges from 23.5 to 18.7 meV as listed in Table I. A sufficiently small recoil energy was further validated from the HR VB spectrum for Ce with ΔE = 85 meV, which also showed a clear Fermi edge, as shown in Fig. 1(o).

4.2 3d core-level HAXPES spectra of 4f REs

Figure 2 shows the 3*d* core-level HAXPES spectra of 4*f* RE elemental solids. The 3*d* core-level spectra have shown the spin–orbit splitting ($3d_{5/2}$ and $3d_{3/2}$) and complicated multiplet structures mainly due to the $3d^9 4f^n$ photoemission final states via the exchange interaction between the core–hole and 4*f* electrons. In contrast, the spin–orbit splitting is dominant for $n = 0$ (La) and 14 (Yb and Lu) due to empty and fulfilled 4*f* orbitals, respectively. The broad structures located at the higher E_B side of the $3d_{5/2}$ and $3d_{3/2}$ main peaks are due to the energy loss satellites for La, Yb, and Lu.

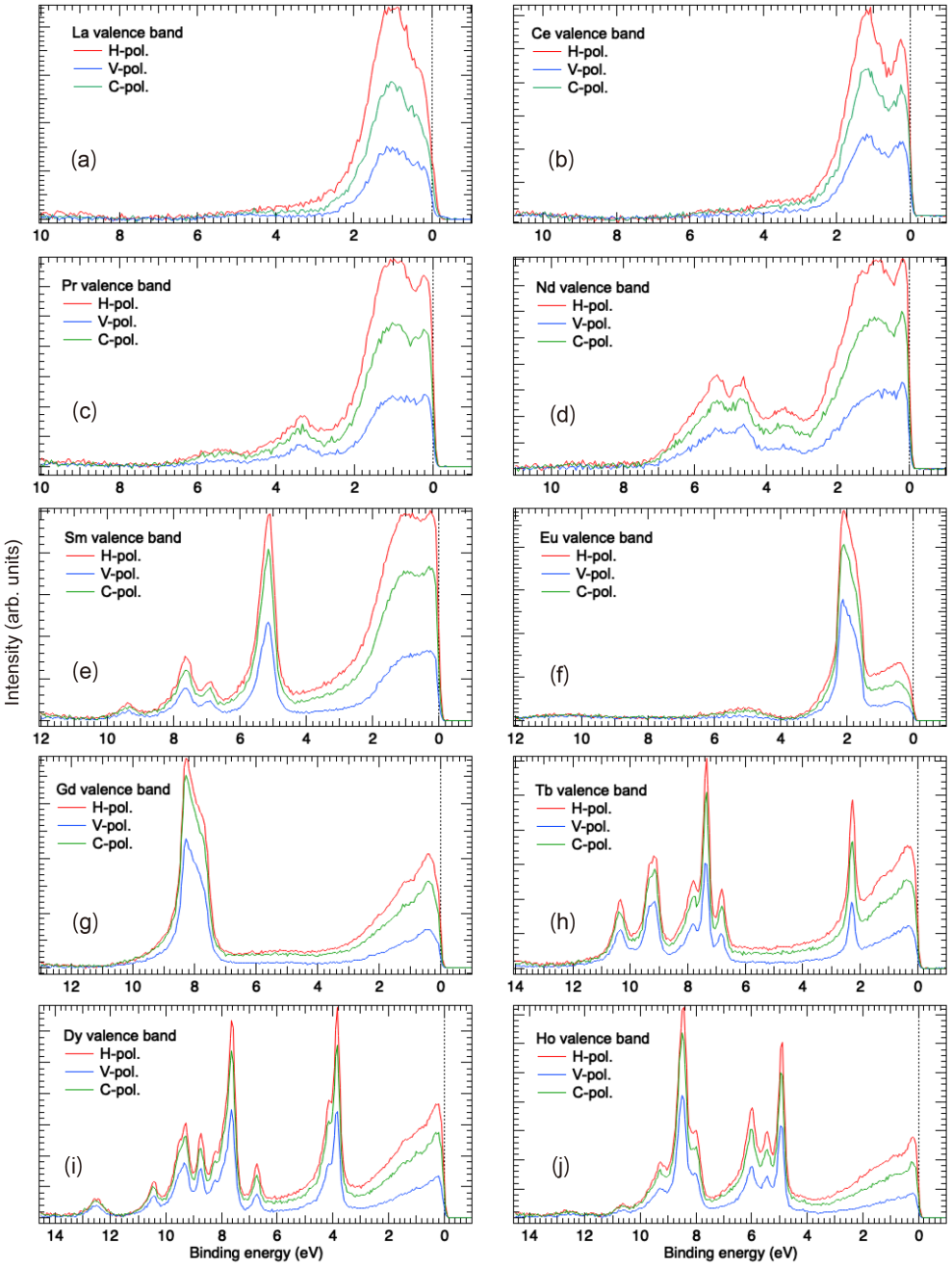

Fig. 1. *Continued on next page.*

Note that conventional XPS measured with Al-Kα (1486.7 eV) or Mg-Kα (1253.6 eV) cannot access to all the 3*d* core-levels in 4*f* REs owing to their high E_B (> 800 eV).

In fact, Ref. 28, which presents the major and high-intensity core-levels in elemental solids, shows the limited 3*d* core-level spectra (La, Ce, Pr, Nd, Sm, and Eu) in 4*f* REs. The observed La, Ce, Pr, Nd, Sm, and Eu 3*d* HAXPES spectra are similar to the reported XPS spectra measured with Al-Kα in Ref. 28 and are sharper than them owing to the HR measurements in this work. Note that in the case of light RE elements, it is known that the experimental spectra are understood by the theoretical calculations based on the impurity Anderson model with taking into account the multiplet states and the charge transfer between 4*f* and conduction electrons and that in the case of heavy RE elements, the ionic model is often applied due to negligible charge transfer effect as described in Ref. 29. In this paper, we do not discuss the charge transfer effects for simplicity, since details of them are described in Ref. 30.

The Eu 3*d* HAXPES spectrum shows several sharp peaks in the $3d_{5/2}$ and $3d_{3/2}$ main structures. A resemblance between the Gd and Eu 3*d* HAXPES spectra is observed, because the spectra mainly reflect the $3d^9 4f^7$ photoemission final states in both Gd and Eu cases. A higher photo-excitation (5.95 keV in this work) enables the observation of the all 3*d* core-level photoemission with high intensity and long probing depth in 4*f* REs. The probing depth (3 × IMFP) for the 3*d* core-level HAXPES in 4*f* REs ranges from 31.8 (La) to 17.1 nm (Lu), where IMFP is calculated by the TPP-2M equation.[11] By utilizing the large probing depth (i.e., high bulk-sensitivity), temperature-induced valence transitions in $YbInCu_4$ and $EuNi_2(Si_{1-x}Ge_x)_2$ have been analyzed

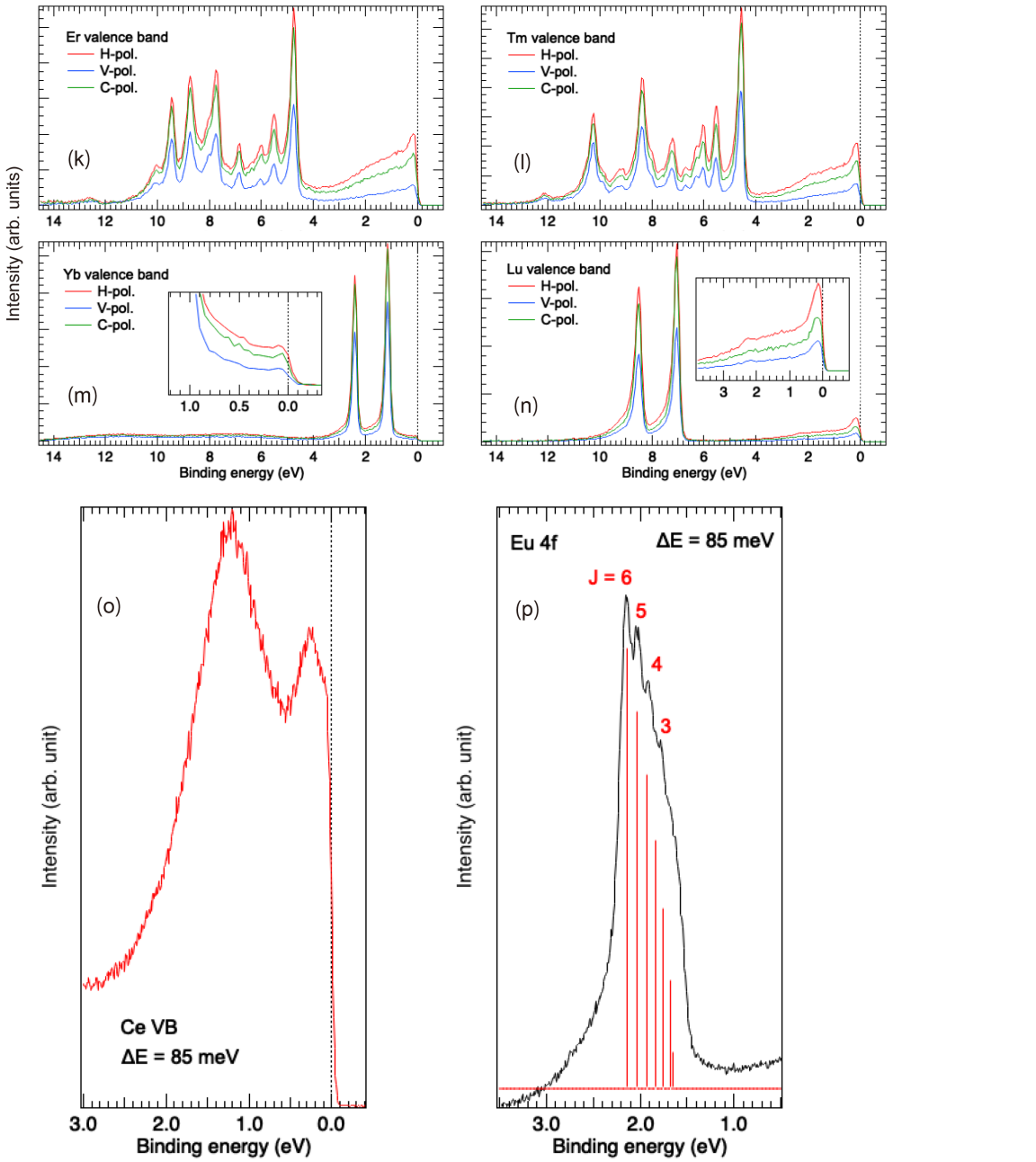

Fig. 1. (Color online) (a)–(n) X-ray polarization-dependent VB HAXPES spectra of La, Ce, Pr, Nd, Sm, Eu, Gd, Tb, Dy, Ho, Er, Tm, Yb, and Lu polycrystalline samples for H-pol (red), V-pol (blue), and C-pol (green) X-rays. In each element, the VB spectra were normalized by the incident X-ray intensity. The insets in (m) and (n) show the enlarged view of the VB spectra near E_F. (o) HR Ce VB HAXPES spectrum and (p) Eu 4*f* spectrum in the case of ΔE = 85 meV. Vertical bars (red) in (p) indicate the multiplet states with different J in the final states.

Table I. Recoil energy of photoelectrons with E_K of 5.95 keV for La, Ce, Pr, Nd, Sm, Eu, Gd, Tb, Dy, Ho, Er, Tm, Yb, and Lu atoms.

Recoil energy (meV)													
La	Ce	Pr	Nd	Sm	Eu	Gd	Tb	Dy	Ho	Er	Tm	Yb	Lu
23.5	23.3	23.2	22.6	21.7	21.5	20.7	20.5	20.1	19.8	19.5	19.3	18.9	18.7

from the Yb and Eu 3*d* core-level HAXPES spectra, respectively.[31,32)]

The observation of the Ce 3*d* core-level spectrum is useful to determine the crystal phase of Ce metal, because α- and γ-Ce shows the different Ce 3*d* XPS spectral shapes.[33)] The observed Ce 3*d* HAXPES spectrum in Fig. 2(b) shows similarity to the Ce 3*d* XPS spectrum for α-Ce rather than γ-Ce according to Ref. 33. For the spectrum of α-Ce, characteristic peaks located at E_B of ~894.7 and ~913.2 eV was found in both the HAXPES and XPS spectra, while these peaks were absent in the 3*d* XPS spectrum of γ-Ce. It is reasonable to assume that the used Ce sample in this work is in the low-temperature α-phase, since the sample was kept at 15 K during the measurements. For Pr metal, the observed 3*d*

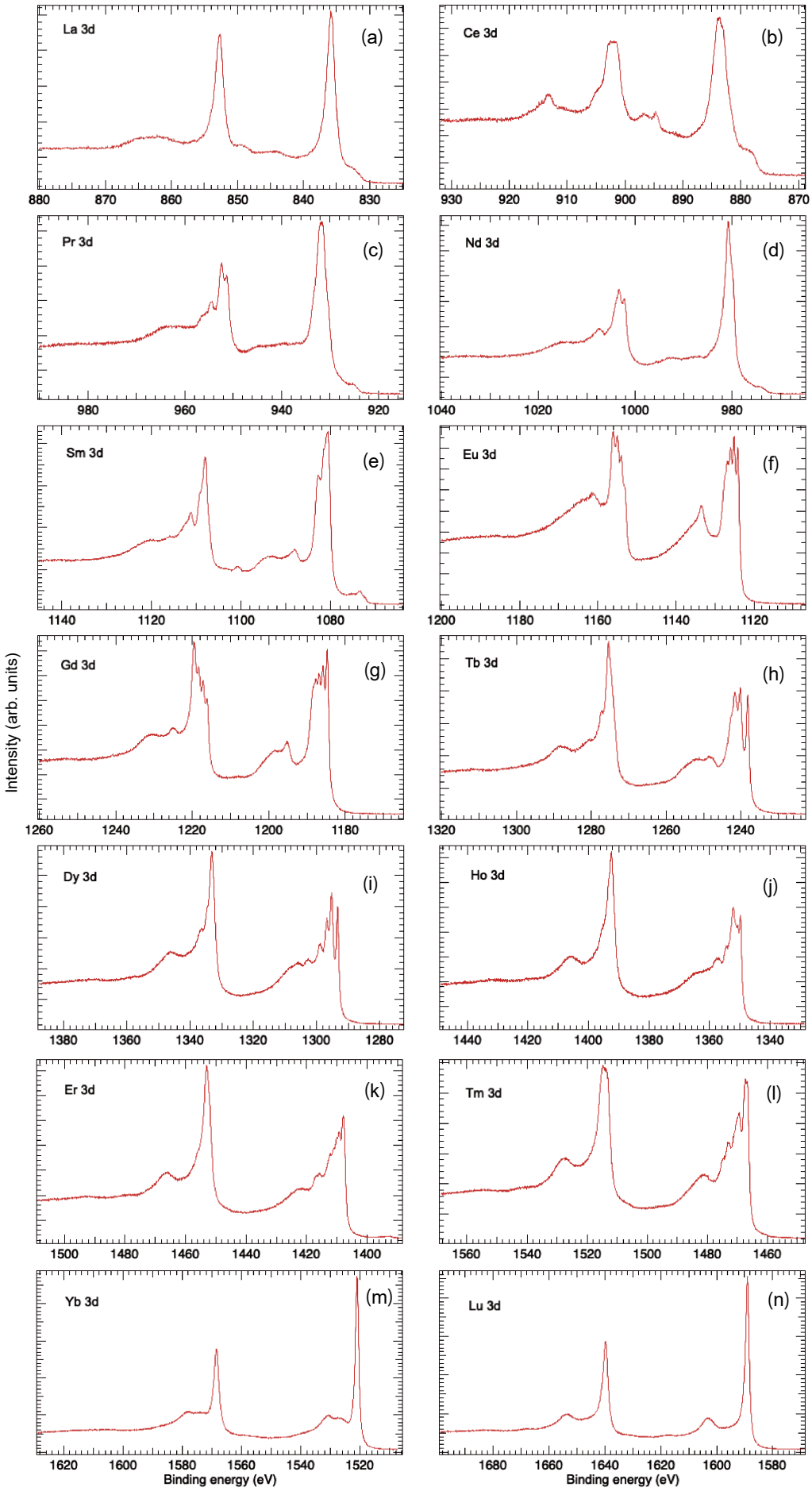

Fig. 2. (Color online) RE 3*d* core-level HAXPES spectra measured with H-pol X-rays.

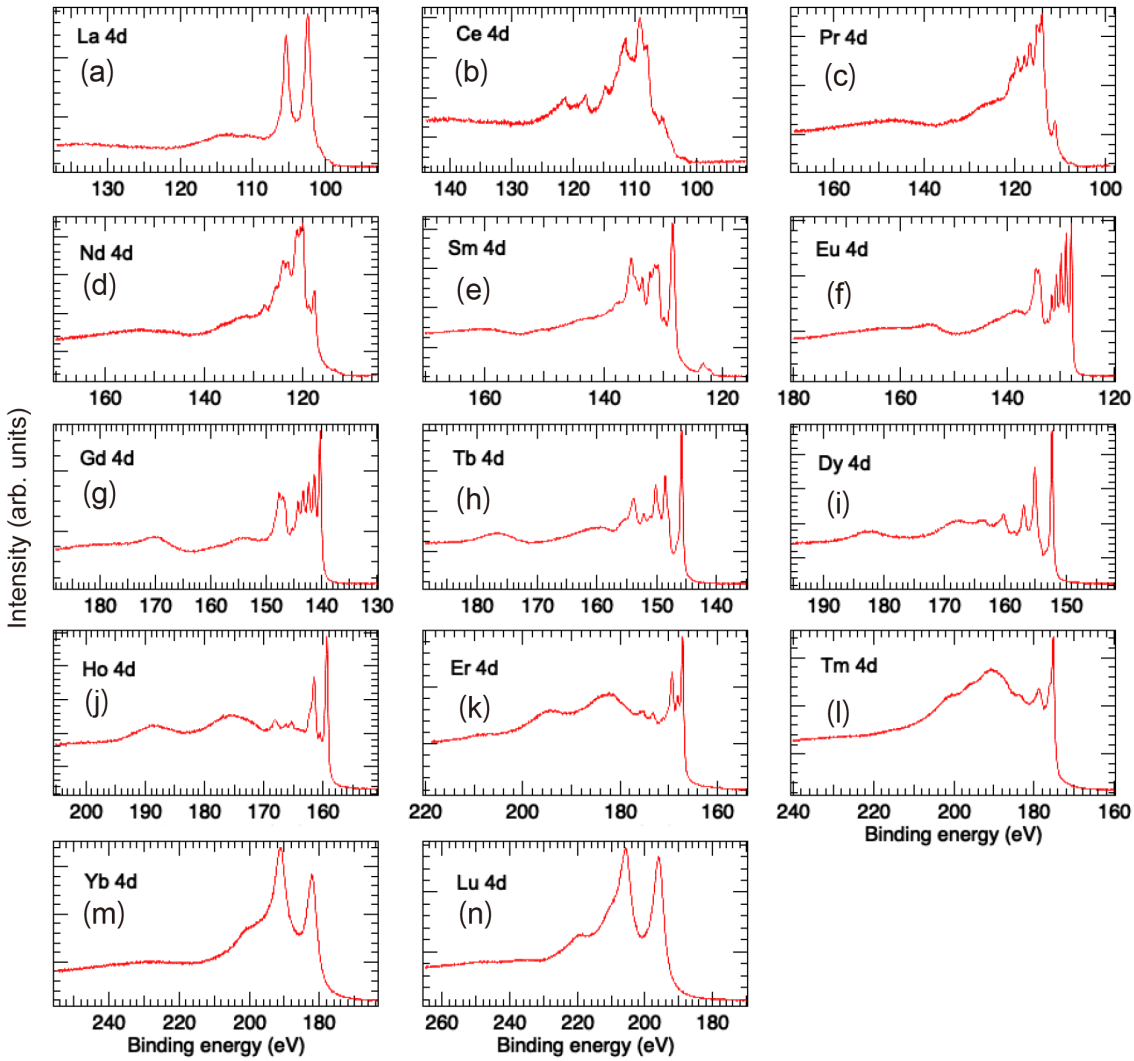

Fig. 3. (Color online) RE 4*d* core-level HAXPES spectra measured with H-pol X-rays.

core-level HAXPES spectrum was similar to the spectra measured with the photon energies of 1253.6, 2450, and 5450 eV in Refs. 34 and 35, suggesting that the E_K dependence on the spectral shape is very weak in Pr metal as well as La, Ce, and Nd metals, which show the resemblance between the HAXPES and the conventional XPS spectra in the 3*d* core-level regions. In contrast, the E_K dependence on the spectral shape for Sm metal is large. The weak peaks located at E_B of ~1073.5 and ~1100.7 eV in the Sm 3*d* core-level HAXPES spectrum increase in the conventional XPS spectra measured with Al-Kα (1486.7 eV) and Mg-Kα (1253.6 eV). Furthermore, as seen in Ref. 28, these peaks are larger in the spectrum for Mg-Kα than that for Al-Kα. Lower E_K for Mg-Kα than Al-Kα corresponds to shorter IMFP for Mg-Kα than Al-Kα according to Ref. 11. This result indicates that these two peaks originate from electronic states near surface of Sm metal, which has been already reported in the take-off-angle dependent Sm 4*d* XPS spectra of Sm metal.[1)]

4.3 4d core-level HAXPES spectra of 4f REs

Figure 3 shows the 4*d* core-level HAXPES spectra of 4*f* RE elemental solids. Owing to higher energy resolution in HAXPES in this work compared to conventional XPS, the 4*d* core-level HAXPES spectra shows fine and complicated multiplet structures mainly due to $4d^9 4f^n$ photoemission final states. The observation of these fine structures is due to less core–hole lifetime broadening in the shallower 4*d* core-levels than the 3*d* core-levels and relatively larger exchange interactions between the core–hole and 4*f* electrons in the 4*d* core-level photoemission process. For La, Yb, and Lu, the spin–orbit doublet ($4d_{5/2}$ and $4d_{3/2}$) is clearly seen in Figs. 3(a), 3(m), and 3(n), while it is not clear in the other 4*f* REs due to their complicated multiplet structures. The broad structure (shoulder) located at the higher E_B side of the $4d_{5/2}$ and $4d_{3/2}$ main peaks is due to the energy loss satellites for La (Yb and Lu). Since E_B of 4*d* core-level region for 4*f* REs is sufficiently lower than the energies of Al-Kα (1486.7 eV) and Mg-Kα (1253.6 eV), conventional XPS can access the all 4*d* core-levels for REs and many 4*d* core-level spectra of the RE elements and oxides have been reported in the early stage of XPS.[28,29,36–38)] In Ref. 29, the experimental 4*d* core-level XPS spectra for Sm, Eu, Gd, Tb, Dy, Ho, Er, Tm, Yb, and Lu metals have been compared with the theoretical multiplet calculations based on the ionic model. The observed 4*d* core-level HAXPES spectra shown in Fig. 4 are much sharper than the reported experimental 4*d* core-level XPS spectra in Refs. 29 and 37 due to the HR HAXPES measurements.

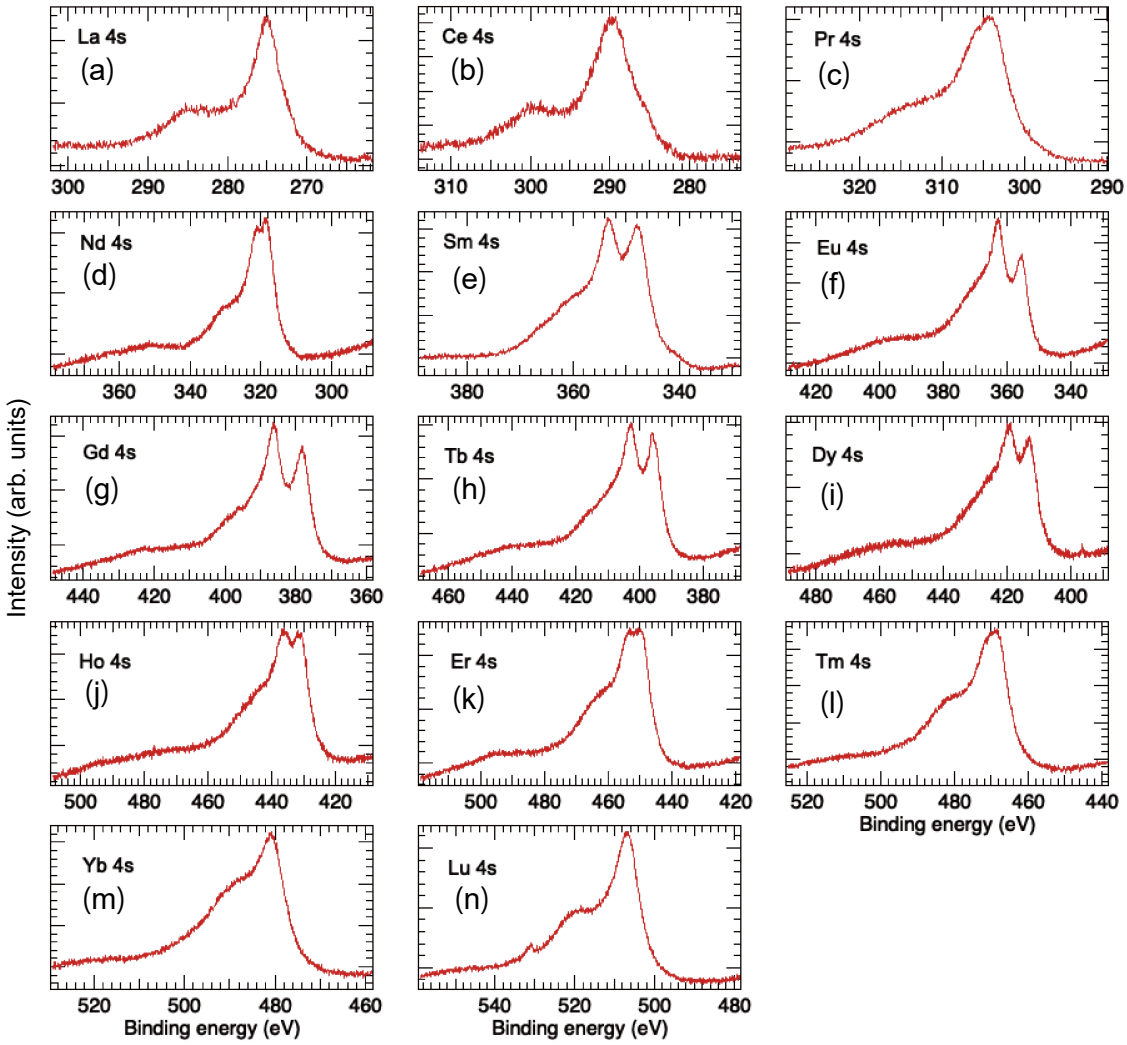

Fig. 4. (Color online) RE 4*s* core-level HAXPES spectra measured with H-pol X-rays.

Note that for Sm, the small peak located at E_B of ~123 eV originates from the electronic state near surface, because of strong reduction in the HAXPES spectrum compared to the XPS one[37] and absence of the small peak in the theoretical calculation,[29] as mentioned above.

In the 4*d* XPS spectra for Ce, Sm, and Eu metals with $\Delta E = 0.55$ eV, fine multiplet structures were observed,[37] but our results on Ce, Sm, and Eu metals with $\Delta E = 130$ meV detected further fine structures. For Eu metal, the impact of ΔE in the spectral shape is apparent; the structure located at E_B of ~130 eV was observed as a broad peak with $\Delta E = 0.7$ eV in Ref. 29, that was observed as several peaks with $\Delta E = 0.55$ eV in Ref. 37, and that was clearly resolved as several sharp peaks in HAXPES with $\Delta E = 130$ meV in this work. Due to the $4d^9 4f^7$ final states in both Eu and Gd metals, the 4*d* core-level HAXPES spectral shapes are similar each other as well as the 3*d* core-level HAXPES cases as shown in Fig. 2. The observed 4*d* core-level HAXPES spectra with $\Delta E = 130$ meV allow the direct comparison with the theoretical multiplet structures indicated by the vertical bars for Sm, Gd, Tb, Dy, Ho, Er, and Tm in Ref. 29. These results indicate the importance of HR measurements of core-level as well as valence band in HAXPES.

4.4 4s core-level HAXPES spectra of 4f REs

Figure 4 shows the 4*s* core-level HAXPES spectra of 4*f* RE elemental solids. It is known that the multiplet structures due to photoemission final states are simplified in the *s* core-level PES spectra and that the spin exchange splitting appears in the *s* core-level spectra due to the interaction between the *s* core–hole and valence electrons.[39] Therefore, the complicated multiplet structures like 3*d* and 4*d* core-level HAXPES spectra are absent in the 4*s* core-level HAXPES spectra for 4*f* REs, and most 4*s* core-level spectra shown in Fig. 4 show the two peaks due to the configuration of core–hole spin parallel or antiparallel to the spin of 4*f* electrons.[40,41] As mentioned in Sect. 1, many RE elemental solids have a magnetic ground state so that the local spin magnetic moment is non-zero, except for La (empty 4*f* orbital) and Yb and Lu (fulfilled 4*f* orbital). Therefore, the peak splitting in the 4*s* spectra due to the spin exchange interaction between the 4*s* core–hole and 4*f* electrons can be clearly seen in Sm, Eu, Gd, Tb, Dy, and Ho metals, while the peak splitting is unclear or small in Ce, Pr, Nd, Er, and Tm metals due to their small spin magnetic moments. One sees that the 4*s* core-level HAXPES spectra of 4*f* RE metals in Fig. 4 show clear shoulder structures at the higher E_B side of two peaks (Nd, Sm, Eu, Gd, Tb, Dy, Ho, and Er) or main peak (La, Ce, Pr, Tm, Yb, and Lu). Note that

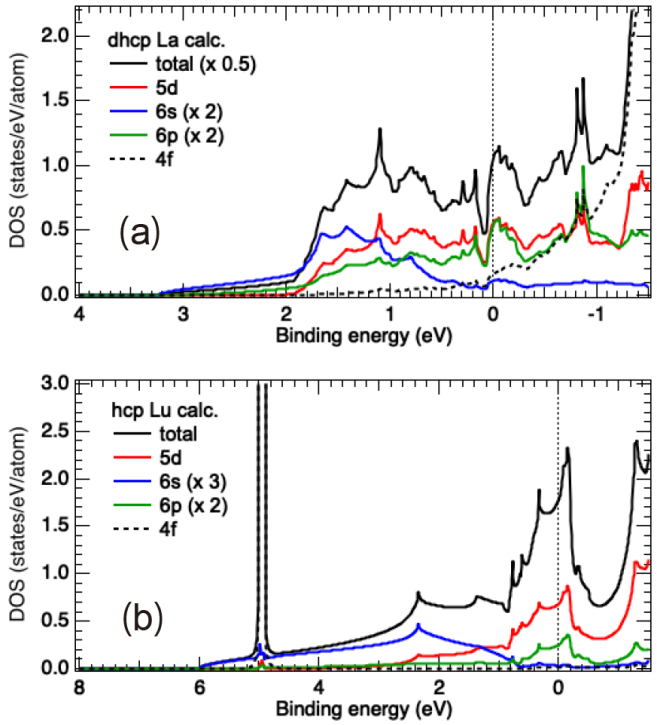

Fig. 5. (Color online) Total DOSs and 5*d*, 6*s*, 6*p*, and 4*f* PDOSs for (a) dhcp La and (b) hcp Lu obtained from the DFT calculations.

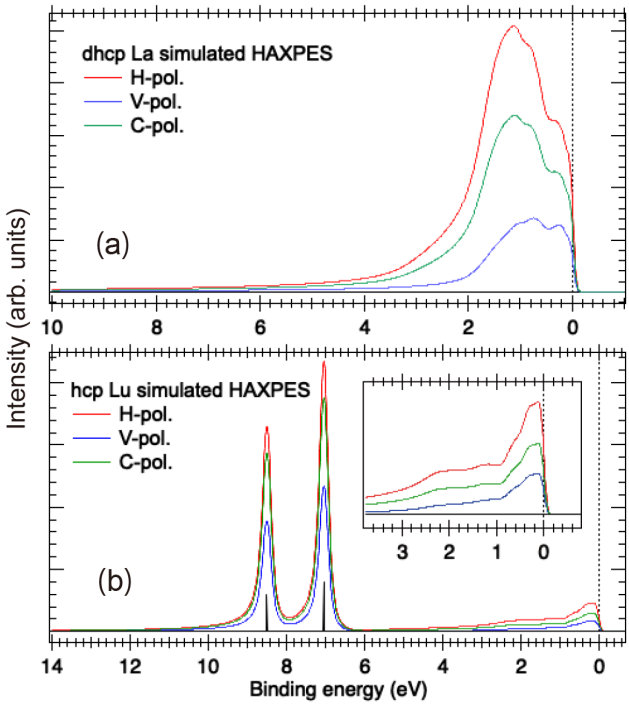

Fig. 6. (Color online) Simulated X-ray polarization-dependent VB spectra for (a) La and (b) Lu. The red (blue) [green] solid curves indicate H-pol (V-pol) [C-pol] X-rays. Note that in the simulation for Lu, the peak positions of the Lu $4f_{7/2}$ and $4f_{5/2}$ were obtained from Fig. 1(n), and the branching ratio was set to 8 : 6 as indicated by black vertical bars in (b). The inset of (b) shows the enlarged view of the VB spectra near E_F.

a small peak at E_B of ∼531 eV is oxygen-related surface contaminations for Lu. The shoulder structures in Fig. 4 seem to be absent in the 4*s* XPS for insulating RE trifluoride.[41] Thus, the shoulder structures in the 4*s* HAXPES spectra for 4*f* RE metals originate from the energy loss satellites due to plasmon excitations. The relatively large intensity of the energy loss satellite in the 4*s* HAXPES suggests that the presence of the energy loss satellite at the higher E_B side of the main structure in the 3*d* and 4*d* HAXPES spectra in the case of 4*f* RE metals. A series of 3*d*, 4*d*, and 4*s* core-level HAXPES measurements, thus, provides information on the energy loss satellite in the core-level spectra for 4*f* RE metals and suggests the necessity of considering the energy loss satellite in the analysis of core-level spectra based on the ionic model in metallic RE alloys and compounds.

5. Discussion

To understand the electronic structures of 4*f* RE elemental solids from the VB HAXPES measurements, we have performed the DFT calculations to obtain the total DOS and PDOSs as shown in Fig. 5. Since the DFT calculations generally do not give the photoemission final states, we focused on the RE elements with $n = 0$ (La) and 14 (Lu) to exclude the 4*f* contribution to the DOS. As seen in Fig. 5, the 5*d* PDOS mainly contributes to the DOS in each case. The 4*f* contribution to the occupied states in La is negligibly small as seen in Fig. 5(a), while the 4*f* states are localized as a shallow core-level at E_B of ∼4.9 eV in Lu as seen in Fig. 5(b). Figure 6 shows the simulated VB HAXPES spectra for various X-ray polarization for La and Lu. In the simulations, the sum of the 5*d* and 6*s* PDOSs multiplied by the photoionization cross-sections per electron with taking the orbital-dependent angular distributions with respect to the X-ray polarizations into account was used, while the 6*p* PDOS was ignored probably due to a quite small cross-section in RE atoms as expected from a quite small 6*p* cross-section in 5*d* TMs.[15] In addition, the 4*f* PDOSs for La and Lu obtained by the DFT calculations were not used in the simulations. The simulated VB HAXPES spectra for La and Lu in Figs. 6(a) and 6(b) reproduced well the experimental polarization-dependent VB HAXPES spectra in Figs. 1(a) and 1(n), respectively. Therefore, the X-ray polarization-dependent VB spectral shape can be understood by the changes in the cross-section ratio with considering the angular distribution of 5*d* orbital to 6*s* one. The calculated 6*s* and 4*f* cross-sections with respect to 5*d* one for RE atoms for 6 keV photoexcitation[42–44] with taking the angular distributions with respect to the X-ray polarizations into account are summarized in Table II. The calculated 5*d* cross-section ratios of RE atoms with respect to La 5*d* one are also summarized in Table III. The drastic changes in the 6*s* cross-section between H- and V-pol in our experimental geometry seen in Table II reflect the changes in the VB profile at E_B of ∼1.5 eV (2.2 eV) for La (Lu). This result is consistent with the fact that the PDOS calculations show that the broad 6*s* states locate at around E_B of ∼1.5 eV (∼2.2 eV) for La (Lu) and that the relatively narrow 5*d* states locate near E_F in both La and Lu. These changes in the experimental band profiles derived from the 5*d* and 6*s* states for the other REs were also reproduced by tentative simulations as mentioned in Appendix, except for Eu and Yb.

Next, we discuss the 4*f* states in the VB region of Ce metal. In Fig. 1(b), it is hard to find the 4*f* photoemission signal for Ce in HAXPES, although a small hump at E_B of ∼3.3 eV due to the 4*f* photoemission signal for Pr can be seen

Table II. Polarization-dependent cross-sections per electron of 5*d*, 4*f*, 6*s* orbitals for isolated La, Ce, Pr, Nd, Sm, Eu, Gd, Tb, Dy, Ho, Er, Tm, Yb, Lu atoms for H-, V-, and C-pol X-rays at the photon energy of 6 keV. The 5*d* cross-sections were obtained by the interpolation of those for La, Gd, and Lu. The 6*s* cross-section for Ce was obtained by the extrapolation of those for the other REs. The values were normalized by that of the 5*d* orbital in each element for H-pol X-rays. Note that the orbital-dependent angular distributions with respect to the X-ray polarizations were taken into account in the polarization-dependent cross-sections in the table.

Element	H-pol.			V-pol.			C-pol.		
	5*d*	4*f*	6*s*	5*d*	4*f*	6*s*	5*d*	4*f*	6*s*
La	1.000	—	1.4935	0.2405	—	0.01880	0.6086	—	0.7483
Ce	1.000	0.1917	1.1898	0.2336	0.0899	0.01549	0.6056	0.1351	0.5962
Pr	1.000	0.2273	1.1306	0.2247	0.1047	0.01518	0.6017	0.1594	0.5667
Nd	1.000	0.2670	1.0807	0.2170	0.1201	0.01328	0.5983	0.1858	0.5409
Sm	1.000	0.3558	0.9868	0.2043	0.1557	0.01443	0.5927	0.2461	0.4948
Eu	1.000	0.4069	0.9476	0.1990	0.1754	0.01438	0.5904	0.2808	0.4753
Gd	1.000	0.4942	1.0516	0.1994	0.2097	0.01637	0.5905	0.3397	0.5276
Tb	1.000	0.5244	0.8799	0.1900	0.2188	0.01415	0.5864	0.3588	0.4416
Dy	1.000	0.5915	0.8504	0.1861	0.2426	0.01413	0.5847	0.4030	0.4269
Ho	1.000	0.6645	0.8232	0.1826	0.2680	0.01411	0.5832	0.4508	0.4134
Er	1.000	0.7435	0.7980	0.1793	0.2951	0.01421	0.5818	0.5024	0.4009
Tm	1.000	0.8297	0.7747	0.1764	0.3238	0.01431	0.5805	0.5583	0.3894
Yb	1.000	0.9219	0.7531	0.1737	0.3546	0.01441	0.5793	0.6182	0.3787
Lu	1.000	1.0950	0.8898	0.1690	0.4154	0.01762	0.5773	0.7318	0.4477

Table III. Relative per-electron cross-sections of the La, Ce, Pr, Nd, Sm, Eu, Gd, Tb, Dy, Ho, Er, Tm, Yb, and Lu 5*d* orbitals to that of the La 5*d* orbital for H-pol X-rays at the photon energy of 6 keV. Note that the cross-section ratio (Ti 3*d*/La 5*d*) is 0.01481.

Relative cross-section of 5*d* orbitals													
La	Ce	Pr	Nd	Sm	Eu	Gd	Tb	Dy	Ho	Er	Tm	Yb	Lu
1.0000	1.0997	1.1829	1.2662	1.4328	1.5160	1.6324	1.6826	1.7658	1.8491	1.9324	2.0157	2.0989	2.1658

in Fig. 1(c). If the 4*f* photoemission signal for Ce is detectable in HAXPES, a sharp peak structure located near E_F can be found as observed in Ref. 45. To clarify whether the 4*f* photoemission signal is detectable, we have performed the HR HAXPES measurement for Ce using H-pol X-rays as shown in Fig. 1(o). The observed spectrum with $\Delta E = 85$ meV was sharper than that with $\Delta E = 130$ meV for H-pol X-rays, but a peak at $E_B \sim 2$ eV due to the $4f^1$-to-$4f^0$ photoemission process and a sharp peak (a tail of Kondo resonance peak) in the vicinity of E_F in α-Ce (low-temperature phase) reported in Ref. 45 cannot be found. On the other hand, these two structures can be seen in the XPS spectrum for Ce (high-temperature γ-phase), even though their intensities are weak compared to the photoemission intensity derived from the Ce 5*d* states.[23] This fact suspects that the photoionization cross-section ratio of 4*f*/5*d* orbitals in HAXPES (5.95 keV) is much smaller than that in XPS (1486.7 eV). The calculated cross-section ratios of 4*f*/5*d* orbitals are ~0.19 and ~1.16 for HAXPES and XPS in the same experimental geometry, respectively.[46] The absence of the 4*f* related peaks even in HR-HAXPES might lead that the calculated cross-section ratio of 4*f*/5*d* orbitals for 6 keV is overestimated, since the 4*f*/5*d* ratio of ~0.19 is not so small to detect the 4*f* related peaks. These results suggest that the direct observation of Ce 4*f* photoemission is in a difficult situation for HAXPES due to a quite smaller 4*f* cross-section compared to 5*d* one and the condition of $n = 1$ for Ce.

Finally, we mention the impact of the HR measurement in HAXPES. Figure 1(p) shows the Eu 4*f* HAXPES spectrum with $\Delta E = 85$ meV for H-pol X-rays. The fine multiplet structures due to the $4f^7$-to-$4f^6$ photoemission process were observed. The multiplet states for $J = 6$, 5, and 4 deduced from the theoretical calculations[24] were found as distinguishable peaks in the experimental spectrum, while that for $J = 3$ appeared as a shoulder structure. These peaks were not resolved in the VB spectrum with $\Delta E = 130$ meV as seen in Fig. 1(f) and the simulated Eu 4*f* spectrum for $\Delta E = 130$ meV as shown in Fig. A·1(e) for H-pol X-rays. Whether the recoil effects[25–27] in high E_K photoelectrons exist (e.g., the energy shift as listed in Table I and broadening of spectral shape) in 4*f* RE elemental solids, the result of the Eu 4*f* HAXPES spectrum shown in Fig. 1(p) strongly suggests the importance of HR measurements in HAXPES to elucidate the electronic states of materials at least photo-excitation (or E_K of photoelectrons) up to 6 keV, which is also supported by the fine and complicated multiplet structures for 4*f* REs in the 3*d* and 4*d* core-level HAXPES spectra as seen in Figs. 2 and 3.

6. Summary

We have conducted the VB, 3*d*, 4*d*, and 4*s* core-level measurements of the elemental solids of 4*f* REs (La, Ce, Pr, Nd, Sm, Eu, Gd, Tb, Dy, Ho, Er, Tm, Yb, and Lu) by means of bulk-sensitive HAXPES with $\Delta E = 130$ meV. The VB spectra for 4*f* REs were separated by 5*d*6*sp*-derived band located near E_F and multiplet structure due to the 4*f* photoemission final states, while the 4*f* photoemission intensity was not found for La and Ce. The absence of the 4*f* signal in La is due to $n = 0$ (the empty 4*f* level), but the absence of the 4*f* signal in Ce with $n = 1$ even in the HR measurement ($\Delta E = 85$ meV) is due to the quite low photoionization cross-section ratio of 4*f*/5*d* orbitals. For Yb and Lu, the spin–obit doublet ($4f_{7/2}$ and $4f_{5/2}$) was found due to the fully occupied 4*f* level in these metals. The profiles of band near E_F depended on the X-ray polarization in our experimental geometry, while those of the $4f^{n-1}$ multiplet

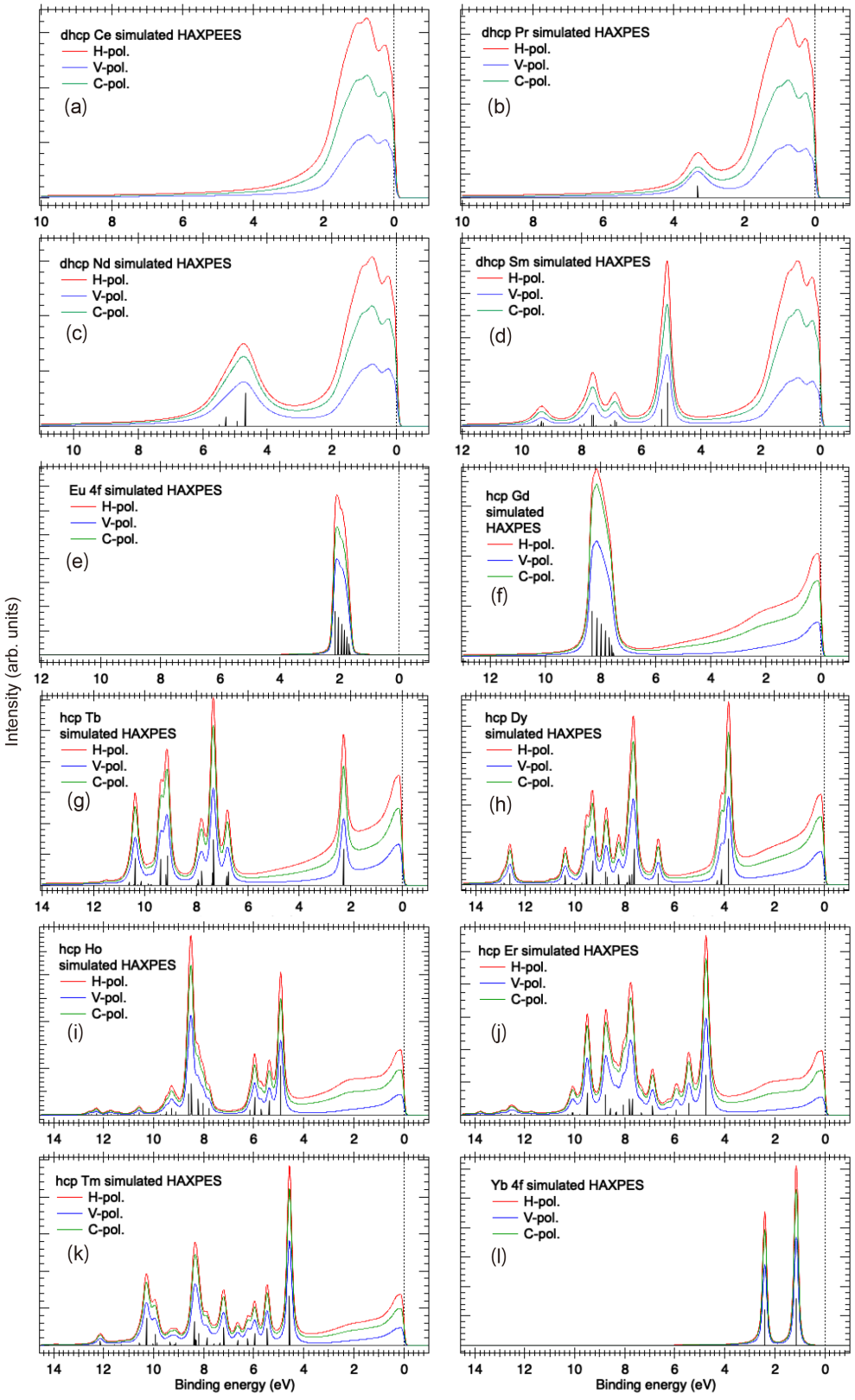

Fig. A·1. (Color online) (a)–(l) Simulated X-ray polarization-dependent VB spectra for Ce, Pr, Nd, Sm, Eu, Gd, Tb, Dy, Ho, Er, Tm, and Yb with 4*f* multiplet final states. For Ce, 4*f* photoemission was excluded, while for Eu and Yb, 5*d*6*s* band photoemission was excluded, for simplicity.

structure did not depend on the X-ray polarization. The changes in the observed band profiles were understood by the X-ray polarization-dependent cross-section ratio of 6*s*/5*d* orbitals.

We have performed the simulations of the polarization-dependent VB spectra near E_F for La and Lu by using the 5*d* and 6*s* PDOSs, which were obtained from the DFT calculations for La and Lu, multiplied by the calculated photoionization cross-sections with considering the angular distributions with respect to the X-ray polarizations. The simulated spectra including the polarization dependence agreed with the experimental spectra for La and Lu. We

have tentatively performed the simulations of the polarization-dependent VB spectra for the other REs by using the PDOSs for La or Lu and photoionization cross-section and the calculated 4*f* multiplet states as shown in Appendix.

The observed 3*d* and 4*d* core-level HAXPES spectra for 4*f* REs showed the complicated multiplet structures via the exchange interaction between the core–hole and 4*f* electrons. In particular, the 4*d* core-level spectra showed fine and complicated structures owing to the HR measurements ($\Delta E = 130$ meV), smaller lifetime broadening effects, and relatively large exchange interactions with the core–hole compared to the 3*d* spectral region. The clear spin exchange splitting in the 4*s* core-level spectra were also observed. Further HR measurement ($\Delta E = 85$ meV) for the Eu 4*f* photoemission revealed that the clear separation of $J = 6$, 5, and 4 states. These results strongly suggest the importance of HR measurements in HAXPES to elucidate the electronic states of materials at least photo-excitation up to 6 keV.

Acknowledgements The HAXPES measurements were performed with the approval of NIMS Synchrotron X-ray Station at SPring-8 (Proposal No. 2019B4606). This work was partially supported from Tokodai Institute for Elemental Strategy (TIES: Grant No. JPMXP0112101001) and Data Creation and Utilization Type Material Research and Development Project (Grant No. JPMXP1122683430) funded by MEXT, Japan.

Appendix: Tentative Simulations of Polarization-dependent VB HAXPES Spectra of REs

In this Appendix, the simulated polarization-dependent VB spectra of Ce, Pr, Nd, Sm, Eu, Gd, Tb, Dy, Ho, Er, Tm, and Yb were shown in Fig. A·1. For Ce, Pr, Nd, and Sm, the PDOSs of dhcp La were tentatively used to calculate the VB photoemission intensity for simplicity. For Gd, Tb, Dy, Ho, Er, and Tm, the PDOSs of hcp Lu were tentatively used to calculate the VB intensity for simplicity. The energy separation and relative photoemission intensity of multiplets states in 4*f* photoemission final states were referred to the theoretical calculation in Ref. 24, except for Ce, Pr, and Yb, and were used in the simulations. Note that the energy separation of the multiplet states was adjusted to the experimental 4*f* spectra. In the case of Ce, the experimental VB spectra did not show the signature of 4*f* photoemission due to lower 4*f* orbital cross-section than 5*d* one as mentioned in Sect. 5. In addition, we tentatively used the 5*d* and 6*s* PDOSs of dhcp La in the simulation for dhcp Ce, while the used Ce sample was in the α-phase. For Pr (Yb), the energy position of single (double) peak(s) due to the 4*f* photoemission was obtained from the experimental VB spectra. The multiplet states were indicated by vertical bars in Fig. A·1. The VB intensity simulation for the 5*d* and 6*s* states was not performed for Eu and Yb by using the 5*d* and 6*s* PDOSs of La or Lu, since the band structure calculations for La and Lu with the $(5d6sp)^3$ configuration were not suitable for Eu and Yb with the $(5d6sp)^2$ configuration. The simulated spectra for the 5*d*6*sp*-derived band agreed with the experimental spectra except the spectral width of 5*d*6*sp*-derived band in later REs probably due to the difference in lattice constant. Overall 4*f* multiplet structures in the experimental spectra agreed with the calculations based on the intermediate coupling model,[24] but the deviation of the intensity ratio between the multiplet components in the present experiments and theory remained, which was also found in later RE elements in Ref. 23, although we did not consider the multiplet-dependent lifetime broadening effects in the simulations. In addition, the agreement between the experiment and calculation for Nd [Figs. 1(d) and A·1(c)] was found to be poor. Since the experimental 4*f* HAXPES spectra in this work reflected bulk-sensitive 4*f* multiplet structures owing to the larger IMFP compared to the previous XPS results,[23] our HR 4*f* spectra could be a useful benchmark for the theoretical approach to the 4*f* photoemission in RE elements.

*Corresponding author. E-mail: UEDA.Shigenori@nims.go.jp

1) *Handbook of the Physics and Chemistry of Rare Earths*, ed. K. A. Gschneidner, Jr., L. Eyring, and S. Hüfner (North-Holland, Amsterdam, 1988) Vol. 10.
2) M. Loewenhaupt and K. H. Fischer, in *Handbook of the Physics and Chemistry of Rare Earths*, ed. K. A. Gschneidner, Jr. and L. Eyring (North-Holland, Amsterdam, 1993) Vol. 16, Chap. 105.
3) *Handbook of Advanced Magnetic Materials*, ed. Y. Liu, D. J. Sellmyer, and D. Shindo (Springer, New York, 2006) Vol. 4.
4) *Handbook of the Physics and Chemistry of Rare Earths*, ed. K. A. Gschneidner, Jr. and L. Eyring (North-Holland, Amsterdam, 2000) Vol. 29.
5) M. B. Maple, in *Handbook of the Physics and Chemistry of Rare Earths*, ed. K. A. Gschneidner, Jr., L. Eyring, and M. B. Maple (North-Holland, Amsterdam, 2000) Vol. 30, Chap. 187.
6) P. Thalmeier and G. Zwicknagl, in *Handbook of the Physics and Chemistry of Rare Earths*, ed. K. A. Gschneidner, Jr., J.-C. G. Bunzli, and V. K. Pecharsky (North-Holland, Amsterdam, 2005) Vol. 34, Chap. 219.
7) Y. Takata, M. Yabashi, K. Tamasaku, Y. Nishino, D. Miwa, T. Ishikawa, E. Ikenaga, K. Horiba, S. Shin, M. Arita, K. Shimada, H. Namatame, M. Taniguchi, H. Nohira, T. Hattori, S. Sodergren, B. Wannberg, and K. Kobayashi, Nucl. Instrum. Methods Phys. Res., Sect. A **547**, 50 (2005).
8) K. Kobayashi, M. Yabashi, Y. Takata, T. Tokushima, S. Shin, K. Tamasaku, D. Miwa, T. Ishikawa, H. Nohira, T. Hattori, Y. Sugita, O. Nakatsuka, S. Sakai, and S. Zaima, Appl. Phys. Lett. **83**, 1005 (2003).
9) S. Ueda, J. Electron Spectrosc. Relat. Phenom. **190**, 235 (2013).
10) C. S. Fadley, J. Electron Spectrosc. Relat. Phenom. **190**, 165 (2013).
11) S. Tanuma, C. J. Powell, and D. R. Penn, Surf. Interface Anal. **21**, 165 (1994); S. Tanuma, C. J. Powell, and D. R. Penn, Surf. Interface Anal. **43**, 689 (2011).
12) S. Ueda, Appl. Phys. Express **11**, 105701 (2018).
13) S. Ueda and I. Hamada, J. Phys. Soc. Jpn. **86**, 124706 (2017).
14) S. Ueda and I. Hamada, J. Phys. Soc. Jpn. **90**, 034706 (2021).
15) S. Ueda and I. Hamada, J. Phys. Soc. Jpn. **91**, 024801 (2022).
16) S. Ueda, Y. Katsuya, M. Tanaka, H. Yoshikawa, Y. Yamashita, S. Ishimaru, Y. Matsushita, and K. Kobayashi, AIP Conf. Proc. **1234**, 403 (2010).
17) P. E. Blöchl, Phys. Rev. B **50**, 17953 (1994).
18) G. Kresse and J. Furthmüller, Phys. Rev. B **54**, 11169 (1996).
19) G. Kresse and D. Joubert, Phys. Rev. B **59**, 1758 (1999).
20) J. P. Perdew, K. Burke, and M. Ernzerhof, Phys. Rev. Lett. **77**, 3865 (1996).
21) D. A. Papaconstantopoulos, *Handbook of the Band Structure of Elemental Solids* (Springer, New York, 2015) 2nd ed., Chap. 13.
22) F. H. Spedding, A. H. Daane, and K. W. Herrmann, Acta Crystallogr. **9**, 559 (1956).
23) J. K. Lang, Y. Bear, and P. A. Cox, J. Phys. F **11**, 121 (1981).
24) F. Gerken, J. Phys. F **13**, 703 (1983).
25) Y. Takata, Y. Kayanuma, M. Yabashi, K. Tamasaku, Y. Nishino, D. Miwa, Y. Harada, K. Horiba, S. Shin, S. Tanaka, E. Ikenaga, K. Kobayashi, Y. Senba, H. Ohashi, and T. Ishikawa, Phys. Rev. B **75**, 233404 (2007).
26) Y. Takata, Y. Kayanuma, S. Oshima, S. Tanaka, M. Yabashi, K. Tamasaku, Y. Nishino, M. Matsunami, R. Eguchi, A. Chainani, M. Oura, T. Takeuchi, Y. Senba, H. Ohashi, S. Shin, and T. Ishikawa, Phys. Rev. Lett. **101**, 137601 (2008).

27) S. Suga, A. Sekiyama, H. Fujiwara, Y. Nakatsu, T. Miyamachi, S. Imada, P. Baltzer, S. Niitaka, H. Takagi, K. Yoshimura, M. Yabashi, K. Tamasaku, A. Higashiya, and T. Ishikawa, New J. Phys. **11**, 073025 (2009).
28) *Handbook of X-ray Photoelectron Spectroscopy*, ed. J. Chastain and R. C. King, Jr. (Physical Electronics, Chanhassen, MN, 1993).
29) H. Ogasawara, A. Kotani, and B. T. Thole, Phys. Rev. B **50**, 12332 (1994).
30) F. de Groot and A. Kotani, *Core Level Spectroscopy of Solids* (CRC Press, Boca Raton/London/New York, 2008).
31) H. Sato, K. Shimada, M. Arita, K. Hiraoka, K. Kojima, Y. Takeda, K. Yoshikawa, M. Sawada, M. Nakatake, H. Namatame, M. Taniguchi, Y. Takata, E. Ikenaga, S. Shin, K. Kobayashi, K. Tamasaku, Y. Nishino, D. Miwa, M. Yabashi, and T. Ishikawa, Phys. Rev. Lett. **93**, 246404 (2004).
32) K. Ichiki, K. Mimura, H. Anzai, T. Uozumi, H. Sato, Y. Utsumi, S. Ueda, A. Mitsuda, H. Wada, Y. Taguchi, K. Shimada, H. Namatame, and M. Taniguchi, Phys. Rev. B **96**, 045106 (2017).
33) E. Wuillound, H. R. Moser, W.-D. Schneider, and Y. Bear, Phys. Rev. B **28**, 7354 (1983).
34) H. Ishii, K. Obu, M. Shinoda, C. Lee, Y. Takayama, T. Miyahara, T. D. Matsuda, H. Sugawara, and H. Sato, J. Phys. Soc. Jpn. **71**, 156 (2002).
35) A. Sekiyama, S. Imada, A. Yamasaki, and S. Suga, in *Very High Resolution Photoelectron Spectroscopy*, ed. S. Hüfner (Springer, Berlin/Heidelberg, 2007) Lecture Notes in Physics, Vol. 715, Chap. 13.
36) J. C. Fuggle, F. U. Hillebrecht, Z. Zonlnierek, R. Lässer, Ch. Freiburg, O. Gunnarsson, and K. Schönhammer, Phys. Rev. B **27**, 7330 (1983).
37) S. P. Kowalczyk, N. Edelstein, F. R. McFeely, L. Ley, and D. A. Shirley, Chem. Phys. Lett. **29**, 491 (1974).
38) A. Kotani and H. Ogasawara, J. Electron Spectrosc. Relat. Phenom. **60**, 257 (1992).
39) S. Hüfner, *Photoelectron Spectroscopy* (Springer, Berlin/Heidelberg/New York, 2003) 3rd ed.
40) F. R. McFeely, S. P. Kowalczyk, L. Ley, and D. A. Shirley, Phys. Lett. A **49**, 301 (1974).
41) R. L. Cohen, G. K. Wertheim, A. Rosencwaig, and H. J. Guggenheim, Phys. Rev. B **5**, 1037 (1972).
42) M. B. Trzhaskovskkaya, V. I. Nefedov, and V. G. Yarzhemsky, At. Data Nucl. Data Tables **77**, 97 (2001).
43) M. B. Trzhaskovskaya, V. K. Nikulin, V. I. Nefedov, and V. G. Yarzhemsky, At. Data Nucl. Data Tables **92**, 245 (2006).
44) J. H. Scofield, Lawrence Livermore Laboratory, Tech. Rep. UCRL-51326 (1973).
45) K. Shimada, in *Very High Resolution Photoelectron Spectroscopy*, ed. S. Hüfner (Springer, Berlin/Heidelberg, 2007) Lecture Notes in Physics, Vol. 715, Chap. 4.
46) J. J. Yeh and I. Lindau, At. Data Nucl. Data Tables **32**, 1 (1985).